IAEA
INTERNATIONAL ATOMIC ENERGY AGENCY

22nd IAEA Fusion Energy Conference

Geneva, Switzerland, 13-18 October 2008

IAEA-CN-165 / TH / 8-3

Gyrokinetic simulations of impurity, He ash and α particle transport and consequences on ITER transport modelling

C. Angioni[1], A.G. Peeters[2], G.V. Pereverzev[1], A. Bottino[1], J. Candy[3], R. Dux[1], E. Fable[4], T. Hein[1], R.E. Waltz[3]

[1] Max-Planck-Institut für Plasmaphysik, EURATOM Association, D-85748 Garching, Germany
[2] Center for Fusion, Space and Astrophysics, Physics department, University of Warwick, CV4 7AL, Coventry UK
[3] General Atomics, San Diego, California 92121
[4] Centre de Recherches en Physique des Plasmas, Association Euratom–Confédération Suisse, EPFL, 1015 Lausanne, Switzerland

Gyrokinetic simulations of impurity, He ash and α particle transport and consequences on ITER transport modelling

C. Angioni[1], A.G. Peeters[2], G.V. Pereverzev[1],
A. Bottino[1], J. Candy[3], R. Dux[1], E. Fable[4], T. Hein[1], R.E. Waltz[3]

[1] Max-Planck-Institut für Plasmaphysik, EURATOM Association, D-85748 Garching, Germany
[2] Center for Fusion, Space and Astrophysics, Physics department, University of Warwick, CV4 7AL, Coventry UK
[3] General Atomics, San Diego, California 92121
[4] Centre de Recherches en Physique des Plasmas, Association Euratom–Confédération Suisse, EPFL, 1015 Lausanne, Switzerland
e-mail: Clemente.Angioni@ipp.mpg.de

Abstract This contribution presents theoretical results on the transport of light and heavy impurities, as well as of energetic α particles, produced by the background electrostatic plasma turbulence. Linear and nonlinear simulations with three gyrokinetic codes, GS2, GYRO, and the recently developed GKW, are performed in concert with analytical derivations, in order to elucidate the basic transport mechanisms of impurities and energetic α particles. The relevance of these theoretical results in the transport modelling of the ITER standard scenario is assessed by means of ASTRA simulations, in which the transport of minority species like α particles and He ash is described by means of formulae which fit the gyrokinetic results.

1. Introduction

The study of turbulent transport in tokamak plasmas has been mainly dedicated to the behaviour of heat and particles of electron and main ion species. The behaviour of these main species in normal L–mode and H–mode operation in tokamaks has reached a rather satisfactory level of understanding. This gives some confidence to the predictions of the ITER standard scenario for these plasma species. On the other hand, the behaviour of minority species, like He ash, light and heavy impurities, has received a more limited amount of consideration, although it can have strong impact on the plasma performance, the plasma control and stability.

In this contribution, we present gyrokinetic calculations of impurity transport produced by electrostatic turbulence, mainly connected with ion temperature gradient (ITG) and trapped electron modes (TEM), with particular interest to conditions as those predicted for the ITER standard scenario. In addition, we consider also the transport of energetic α particles produced by the background plasma electrostatic turbulence, in order to establish whether it has to be included in ITER transport modelling or can be neglected.

To this purpose, three gyrokinetic codes, GKW [1], GS2 [2,3] and GYRO [4,5] have been used, in combination with the transport code ASTRA [6]. The latter has been applied for ITER standard scenario transport simulations with the inclusion of the GLF23 transport model [7].

In the next section, general properties of the transport of minority species are identified and expressed in a form easily applicable in transport modelling. In Section 3, linear and nonlinear gyrokinetic simulations of impurity transport are presented. In particular, the experimentally relevant problem of the direction of the impurity convection as a function of the ratio of the electron to ion heat flux and the transport of He ash in H-mode plasma conditions like those predicted for the ITER standard scenario are investigated. Section 4 is dedicated to the study of the transport of energetic α particles. Finally, in Section 5 the relevance of the results presented in the previous Sections in view of ITER transport modelling is discussed.

2. Gyrokinetic description of the transport of minority species

Our study starts from the observation that even within a nonlinear gyrokinetic model, the gyrokinetic equation as such is obviously linear in the distribution function, as any kinetic equation. The nonlinearity in the gyrokinetic model is introduced by the relationships between the

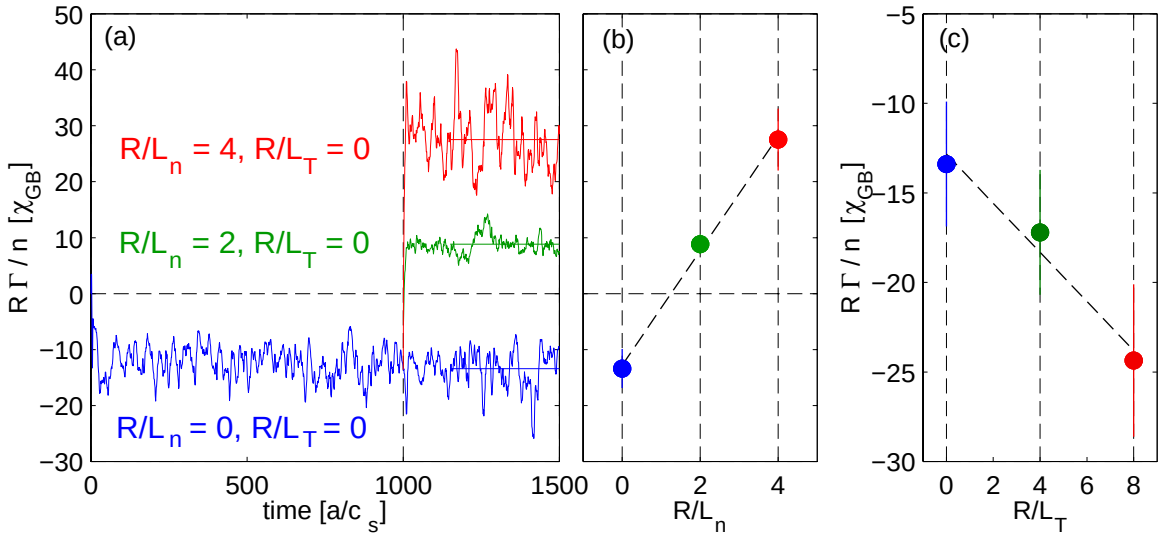

Figure 1: Nonlinear GYRO He flux for different values of the He density (a & b) and temperature (c) logarithmic gradients, as a function of time (a) (restarts are made at 1000 in which the gradients are changed), and as a function of the corresponding gradients (b & c).

potentials and the charge and current distributions in the Poisson and Ampère equations. Within a δf description, in which the distribution function f_σ of the particle species σ, with charge Z_σ, is given by the sum $f_\sigma = \delta f_\sigma + F_{0\sigma}$, the nonlinear gyrokinetic equation for electrostatic fluctuations can be written in the form

$$\frac{\partial h_\sigma}{\partial t} + \mathbf{v}_{gc\sigma}\cdot\nabla h_\sigma + \tilde{\mathbf{v}}_E\cdot\nabla h_\sigma = \mathbf{v}_{gc\sigma}\cdot\nabla\left(Z_\sigma e\frac{\partial F_{0\sigma}}{\partial E}\bar{\phi}\right) - \tilde{\mathbf{v}}_E\cdot\nabla F_{0\sigma}, \tag{1}$$

where the auxiliary perturbed distribution function h_σ is defined as $h_\sigma = \delta f_\sigma - Z_\sigma e(\partial F_{0\sigma}/\partial E)\left(\bar{\phi}-\phi\right)$, and the symbol $\bar{\phi}$ denotes the gyroaverage of the fluctuating electrostatic potential ϕ. In Eq. (1), $\mathbf{v}_{gc\sigma} = \mathbf{v}_{\|} + \mathbf{v}_{d\sigma}$, where $\mathbf{v}_{d\sigma}$ is the combination of the curvature and ∇B drifts, while $\tilde{\mathbf{v}}_E$ is the ExB drift generated by the fluctuating electrostatic potential. The equilibrium distribution function $F_{0\sigma}$ is generally assumed to be a Maxwellian. In Section 3, the case of an unperturbed slowing down distribution function will be considered for the specific application to the problem of energetic particle transport.

In the case that the particle species σ is present in the plasma in a sufficiently small concentration that its contribution to the Poisson equation can be considered negligible, then particles of species σ behave like passive tracers in the plasma and in this case Eq. (1) is a linear equation for h_σ since ϕ, and therefore $\tilde{\mathbf{v}}_E$, are independent of h_σ.

We consider now the case of an unperturbed Maxwellian distribution, and we develop the gradients in the RHS of the equation. Calling $GK(h_\sigma)$ the gyrokinetic operator at the LHS, we obtain,

$$GK(h_\sigma) = -\mathbf{v}_{gc\sigma}\cdot\nabla\left(\frac{Z_\sigma e}{T_\sigma}F_{0\sigma}\bar{\phi}\right) + \tilde{\mathbf{v}}_E\cdot\frac{F_{0\sigma}}{R}\left[\frac{R}{L_{n\sigma}} + \left(\frac{E}{T_\sigma}-\frac{3}{2}\right)\frac{R}{L_{T\sigma}}\right], \tag{2}$$

where we have introduced the normalised logarithmic (radial) gradient of the equilibrium density n_σ and temperature T_σ of species σ, defined as $R/L_{n\sigma} = -R\nabla n_\sigma/n_\sigma$ and $R/L_{T\sigma} = -R\nabla T_\sigma/T_\sigma$, and where the normalisation constant R is the major radius. Within a local description, these gradients are constant numbers in the equation. Since the operator GK is linear, the above equation can be solved formally as follows

$$h_\sigma = -GK^{-1}\left[\mathbf{v}_{gc\sigma}\cdot\nabla\left(\tfrac{Z_\sigma e}{T_\sigma}F_{0\sigma}\bar{\phi}\right)\right] + GK^{-1}\left[\tilde{\mathbf{v}}_E\cdot\frac{F_{0\sigma}}{R}\right]\frac{R}{L_{n\sigma}} + GK^{-1}\left[\left(\frac{E}{T_\sigma}-\frac{3}{2}\right)\tilde{\mathbf{v}}_E\cdot\frac{F_{0\sigma}}{R}\right]\frac{R}{L_{T\sigma}}.$$

Hence, in the case the charge concentration of species σ is small enough, the perturbed distribution function h_σ can be expressed by a functional form which is offset linear in the logarithmic gradients

$$h_\sigma = A_\sigma \frac{R}{L_{n\sigma}} + B_\sigma \frac{R}{L_{T\sigma}} + C_\sigma, \tag{3}$$

where the functions A_σ, B_σ and C_σ are independent of the gradients $R/L_{n\sigma}$ and $R/L_{T\sigma}$, but depend on the mass, charge and temperature of the species σ, as well as on the background plasma parameters of main ions and electrons. It is straightforward to show that such a linear functional form of the perturbed distribution function h_σ implies a linear dependence of the particle and heat fluxes of species σ on the logarithmic gradients $R/L_{n\sigma}$ and $R/L_{T\sigma}$ of the same particle species.

In conclusion, in the most general sense, within a local description, the δf gyrokinetic equation implies that the flux of particles of a particle species σ which is present in small charge concentration has the form

$$\frac{R\Gamma_\sigma}{n_\sigma} = D_\sigma \frac{R}{L_{n\sigma}} + D_{T\sigma} \frac{R}{L_{T\sigma}} + RV_{p\sigma}. \tag{4}$$

The coefficients D_σ, $D_{T\sigma}$ and $RV_{p\sigma}$, which are appropriate flux surface averages of velocity integrals of the functions A_σ, B_σ, C_σ introduced in Eq. (3), have the natural physical interpretation of diffusivity, thermo–diffusivity and pure convection velocity. Eq. (4) provides the most general form of the transport of an impurity, derived from the basic kinetic equation, and perfectly suited to be applied in transport modelling. We introduce the thermodiffusion coefficient $C_{T\sigma} = D_{T\sigma}/D_\sigma$ and convection coefficient $C_{p\sigma} = RV_{p\sigma}/D_{T\sigma}$. In stationary conditions, in the absence of sources, namely for $\Gamma_\sigma = 0$, and in conditions of relatively negligible neoclassical transport, then the logarithmic impurity density gradient produced by the turbulent transport is given by

$$\frac{R}{L_{n\sigma}} = C_{p\sigma} + C_{T\sigma} \frac{R}{L_{T\sigma}}, \tag{5}$$

where, for thermal ionic species $RL_{T\sigma} = RL_{Ti}$, where 'i' stands for the main ion species.

Fig. 1 shows a numerical demonstration of the linear dependence of the particle flux as a function of the logarithmic density and temperature gradients from a set of nonlinear GYRO simulations in which the flux of He in very small charge concentration , namely 3 10^{-4}, has been computed for three different values of the logarithmic density and temperature gradients.

3. Gyrokinetic calculations of impurity transport

Previous studies [8–13] have already identified the main physical mechanisms which are responsible for the different contributions to the total impurity flux. We briefly recall here some basic features [11]. The diffusion coefficient is mainly dominated by the ExB advection and becomes independent of the impurity charge with increasing charge. The thermodiffusion contribution is originated by the coupling between temperature and density fluctuations due to the presence of the curvature and ∇B drifts. As a consequence, the thermodiffusion coefficient C_T decreases with increasing charge and its contribution is usually negligible for heavy impurities. The pure convection term arises from the combination of different mechanisms, both independent of the charge, arising from the compression of the ExB drift, as well as decreasing with charge, due to the curvature and ∇B drifts. In addition, parallel dynamics adds a term dependent on Z/A, where A is the mass of the impurity, which is practically constant for fully ionised impurities, but decreases for very heavy impurities due to incomplete ionisation.

For tokamak operation, conditions in which the total impurity convection is directed outwards are particularly interesting, since they allow the avoidance of central accumulation, with hollow impurity density profiles in the experimental condition of absence of core impurity sources. In addition, in burning plasmas, the magnitude of the He diffusivity governs the impact of the

central He source due to the slowing down of fusion α particles on the He density profile and therefore on central fuel dilution.

Here, we focus on these two aspects of impurity transport, with both linear and nonlinear gyrokinetic simulations. Recent analytical and numerical works based on linear gyrokinetic simulations [11,14] have shown that, due to the contribution due to the parallel dynamics, the pure convection term can reverse direction from inward to outwards for modes propagating in the electron direction. In particular it was found that such a convective mechanism could explain the observed reversal of Si convection measured in AUG in the presence of strong central electron heating [14]. Here, a set of nonlinear flux tube simulations with GYRO are performed in order to assess whether the effect of the reversal of the impurity convection is still at play in nonlinear simulations and at which ratio of the electron to the ion heat flux, pure convection of impurities reverses direction from inward to outward. To this purpose, in these simulations the ratio between ion and electron heat flux has been varied by appropriate variations of the driving gradients. The simulations are electrostatic and collisionless (this does not have big effect on the impurity transport behaviour), with the following parameters, box size $L_x \simeq 80\rho_s$, $L_y \simeq 120\rho_s$, with 160 grid points in the radial direction and 16 toroidal modes, up to $k_\theta\rho_s = 0.84$. The simulation plasma parameters which are kept fixed are $T_e = 2T_i$, $q = 1.4$, $s = 0.8$, $r/R = 0.16$, while the ion and electron temperature gradients are varied in such a way to keep reasonably constant the total heat flux and change the ratio of the electron to the ion heat flux ($T_e > T_i$ is chosen to keep small the contribution from high toroidal mode numbers in simulations with strong electron temperature gradients). Fig. 2 shows the results of these simulations for 4 fully ionised impurities, He, C, Si and Ni. The coefficient C_p is plotted as a function of the charge of the impurity. The impurity convection is directed inward in the case of the simulation in which $Q_e/Q_i = 0.45$ ($R/L_{Te} = R/L_{Ti} = 9$), as well as in the case of the simulation with $Q_e/Q_i = 1.00$ ($R/L_{Te} = 10.2$ and $R/L_{Ti} = 7.5$), while it is directed outwards in the case $Q_e/Q_i = 1.90$ ($R/L_{Te} = 9$ and $R/L_{Ti} = 4.5$). This result shows that the role of the dominant instability as obtained by analytical as well as linear calculations in determining the direction of the impurity convection contribution generated by the parallel compression is confirmed in nonlinear simulations in which the direction of the impurity pinch reverses with increasing ratio of the electron to ion heat flux.

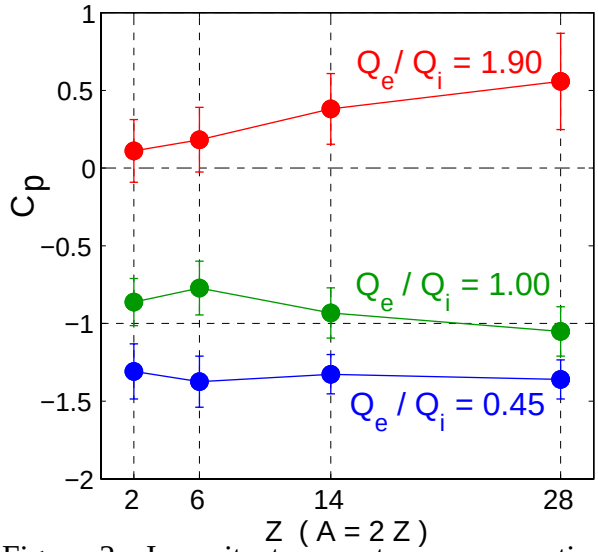

Figure 2: Impurity transport pure convection coefficient C_p as a function of the impurity charge for three different ratios of the electron to ion heat flux, as obtained in GYRO nonlinear gyrokinetic simulations.

Another set of simulations has been performed in order to study He transport in the specific conditions predicted for the standard scenario of ITER. In this case, input parameters for GYRO have been extracted from the plasma profiles obtained by a simulation of the ITER–FEAT standard scenario, applying the ASTRA transport code and the GLF23 transport model. Fig. 5(a) shows the profiles of ion and electron temperatures, electron density, as well as the safety factor, frozen when it reaches one in the center, obtained in this simulation and used for GYRO input. The simulation parameters are $L_x = 80\rho_s$, $L_y = 220\rho_s$, 160 grid points in the radial direction, 32 toroidal modes, with maximum $k_\theta\rho_s = 0.85$. The ion and electron temperature gradients from the GLF23 simulation have been increased, both by the same factor 1.5, in the GYRO input in order to match the total heat flux predicted by the transport simulation at mid-radius.

Fig. 4 shows the results of these simulations for the diffusion coefficient D_{He} as well

as for the thermodiffusion and pure convection coefficients $C_{T\,He}$ and $C_{P\,He}$. We observe that the diffusion coefficient becomes a rather constant function of the minor radius when it is normalised to the total effective conductivity $\chi_{eff} = -2(q_e + q_i)/(n\nabla Te + n\nabla Ti)$F. For similar temperature profiles, as expected in ITER, $\chi_{eff} \simeq \chi_i + \chi_e$. Both the results of nonlinear simulations (full symbols) as well as corresponding linear calculations (open symbols) are shown. These are in good agreement. We find that in these conditions, rather close to marginal stability, the ratio $D_{He}/\chi_{eff} \simeq 1$ all along the minor radius. We underline that while D_{He} is an actual (incremental) diffusivity, χ_{eff} is the effective (power balance) total conductivity of the plasma. The coefficient C_T is found to be positive, namely providing outward thermodiffusion, as it can be expected for prevailing ITG turbulence, as found in these simulations, while the coefficient C_P is negative, namely describing inward pure convection, again consistent with an ITG turbulence. In addition, we have performed a nonlinear simulation with half radius parameters, in which the electron temperature gradient has been increased up to match the ratio of the electron to ion heat flux, namely 1.06, obtained in the ASTRA ITER simulation at that radial location (crossed open symbols). In these conditions, as it can be expected from the results presented in Fig. 2, the coefficient C_P increases from around -2 to greater than -1, and the ratio D_{He}/χ_{eff} increases to 1.5. This simulation, in which the electron to ion flux ratio has been matched, provides more optimistic predictions for He transport in a burning plasma, since it has both higher He diffusion for the same total plasma heat conductivity, as well as reduced inward convection.

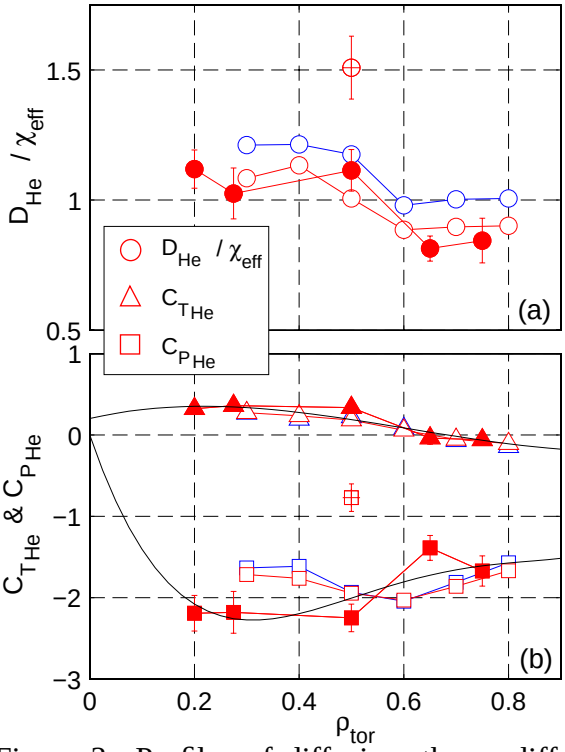

Figure 3: Profiles of diffusion, thermodiffusion and convection coefficients for He from linear (open symbols) and nonlinear (full symbols, crossed open symbols) GYRO simulations, with input data extracted from the ITER profiles predicted by ASTRA with GLF23, and shown in Fig. 5(a).

The scaling $D_{He} = \chi_{eff}$ as well analytical formulae fitting the C_P and C_T profiles obtained in these simulations (solid black lines in Fig. 3), have been included in the ITER modelling with ASTRA. The results will be presented in Section 5.

4. Gyrokinetic calculations of energetic α particle transport

In addition to the study of the transport of He ash, recent results on turbulent transport of energetic particles [15–20] motivate also the assessment of whether electrostatic transport of energetic α particles has to be included in ITER transport modelling or can be safely neglected as usually done. To this purpose we have computed the transport of energetic α particles assuming both a slowing down distribution function, namely

$$F_S = \frac{3\,n_\alpha}{4\pi \ln(v_\alpha^3/v_c^3+1)} \frac{H(v_\alpha - v)}{v_c^3 + v^3}, \qquad (6)$$

as well as an equivalent Maxwellian distribution, namely a Maxwellian distribution whose temperature is equal to the second velocity moment of the slowing down distribution. In Eq. (6), v_α is the maximum fast particle velocity, corresponding to an energy $E_\alpha = m_\alpha v_\alpha^2/2 = 3.5$ MeV for fusion α particles, and v_c is the slowing-down critical velocity (we do not quote here the index

α to lighten the symbols). We note that, when a slowing down distribution is assumed for the equilibrium, then appropriate derivatives with respect to the energy variable E as well as with respect to radial coordinate in the two terms at the right hand side (RHS) of Eq. (1) have to be considered. This has been made and two gyrokinetic codes GS2 and GKW have been modified in order to include properly these terms [21].

In Fig. 4 we plot the diffusivity D_α of the α particles, as defined in Eq. (4), as a function of the electron temperature of the background plasma, and normalised to the corresponding diffusivity D_{He} of He ash, for both particles and heat. These calculations have been performed assuming the following parameters for the background plasma $T_e = T_i$, $R/L_{Te} = R/L_{Ti} = 6$, $R/L_n = 3$, $q = 1.4$, $s = 0.8$ and $r/R = 0.16$. These results have been obtained by utilising three gyrokinetic codes, GKW, GS2, and GYRO, with both the assumptions of Maxwellian and slowing down equilibrium distributions. In addition, the GYRO code has been run both linearly as well as nonlinearly, with a Maxwellian distribution. Nonlinear GYRO simulations have been performed over 16 toroidal modes, and all GYRO simulations have been performed with 16 points on the energy grid. First of all we underline the perfect agreement among codes, linear GYRO and GS2 with a Maxwellian distribution, linear GKW and GS2 with a slowing down distribution. In addition we observe that the difference in the fast particle diffusivity between nonlinear simulations and the corresponding linear ones is below 10 % for all cases studied. Larger differences are observed for the heat diffusivity (dashed lines), in agreement with previous nonlinear simulations in [18]. Of course, relatively to the corresponding thermal transport, the heat transport of energetic α particles is more strongly reduced than the particle transport.

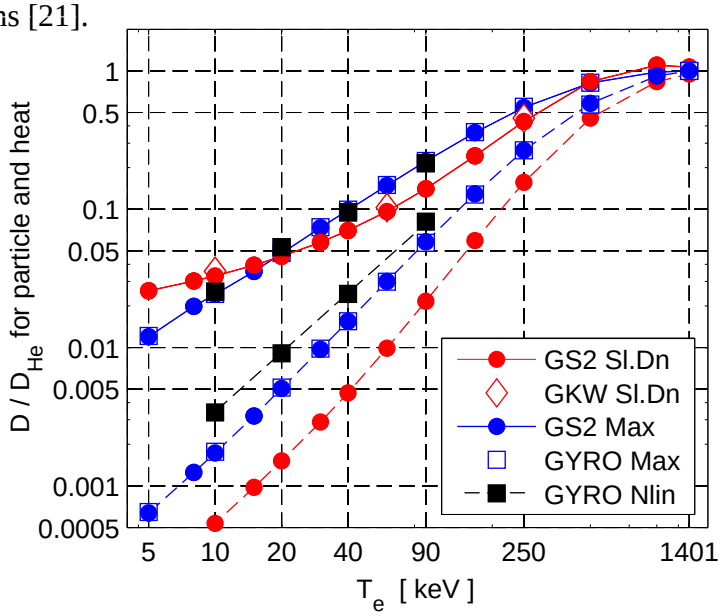

Figure 4: Diffusion coefficient for α particles (solid lines) and heat (dashed lines) normalised to the corresponding thermal value for He, in the case of Maxwellian (blue / black) and slowing down (red) unperturbed distribution functions, computed by linear GS2 (circles), GKW (open diamonds) and GYRO (open squares), as well as nonlinear GYRO (black squares).

Particle transport occurs only in the very low energy range of the distribution. Higher particle diffusivity is obtained at every value of the electron temperature with the equilibrium distribution function which has a larger fraction of particles in the lowest energy range. Interestingly the two curves intersect in the ITER relevant range of 20 keV, since for that electron temperature a slowing down distribution can be almost perfectly approximated with a Maxwellian. We observe that D_α decreases strongly with increasing E_α/T_e, and at plasma temperatures around 20 keV is by at least a factor 20 smaller than the diffusivity of He ash.

The coefficients C_T and C_P for fast α particles are also computed, with both a Maxwellian and a slowing down distribution function. Larger differences have been found on these coefficients, due to the crucial role played by the derivatives of the equilibrium distribution function on these coefficients, as can be inferred from Eq. (2) and Eq. (3) [21]. In particular we note that the radial gradient of the slowing down distribution function Eq. (6) implies that the thermal diffusion term becomes directly proportional to the logarithmic gradient of the background electron temperature, through the gradient of the critical velocity v_c.

Also for fast α particles appropriate formulae, which fit the gyrokinetic results, have been

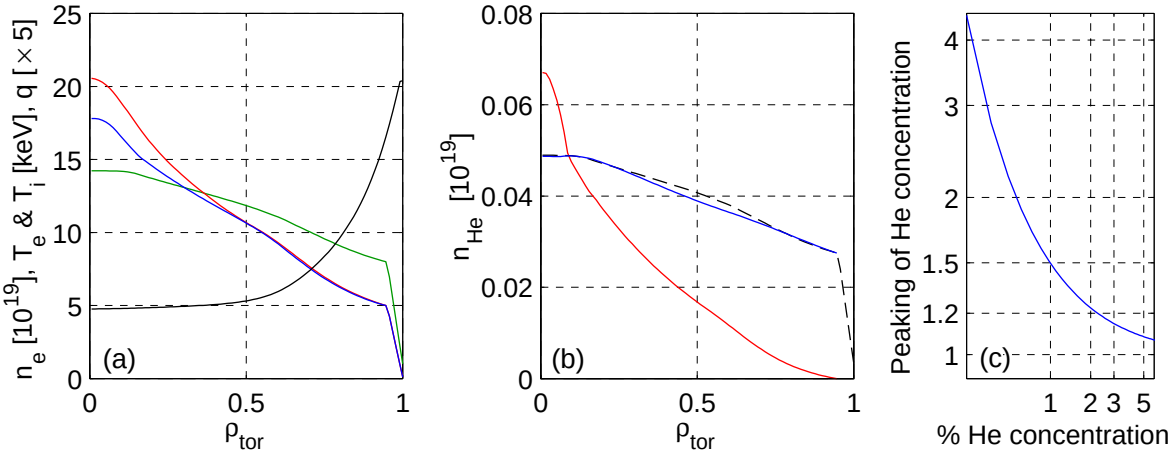

Figure 5: Density, temperature and safety factor profiles of an ASTRA-GLF23 ITER simulations (a), He profiles (b) and peaking of the He concentration profile as a function of the total He concentration (c).

derived [21], and are applied in the next section in ITER modelling with the ASTRA code in order to assess the impact of α transport produced by electrostatic turbulence on the α density profile.

5. Consequences on ITER transport modelling

The gyrokinetic results for He ash and α particle transport have been included in the ITER transport modelling with ASTRA and the GLF23 transport model. The large set of ITER simulations performed in this work in order to test the role of the various transport contributions was possible thanks to the recently developed numerical scheme for stiff transport models [22], which allows one to increase the time step in the transport simulations by at least two orders of magnitude. For the α particle density n_α and He ash density n_{He} we have implemented the following equations in the ASTRA code,

$$\frac{\partial n_\alpha}{\partial t} + \nabla\left(-D_\alpha \nabla n_\alpha + V_\alpha n_\alpha\right) = -\frac{n_\alpha}{\tau^*_{sd}} + n_D n_T \langle\sigma v\rangle_{DT}, \tag{7}$$

$$\frac{\partial n_{He}}{\partial t} + \nabla\left(-D_{He} \nabla n_{He} + V_{He} n_{He}\right) = \frac{n_\alpha}{\tau^*_{sd}}, \tag{8}$$

where $\tau^*_{sd} = \ln(v_\alpha^3/v_c^3+1)\,(m_e m_a v_e^3)/(64\sqrt{\pi}e^4 n_e \ln\Lambda)$ is the actual thermalization slowing down time, obtained from the zero order energy moment of the Fokker–Planck equation, with v_e the electron thermal velocity. Fig. 5(a) shows the ion and electron temperatures, electron density, as well as the safety factor obtained in the ASTRA simulation of ITER FEAT with GLF23. Also the electron density profile has been simulated, fulfilling the condition of zero particle flux in the plasma core [23]. The transport of energetic α particles is included by formulae which fit the gyrokinetic results [21]. We find that the transport of α particles produced by electrostatic turbulence has negligible effect on the α density profile, and leads to particle losses which do not exceed 1%. In case the transport of α particles is assumed to be 10 times or 100 times larger than the theoretical predictions, then the transport of α particles becomes visible, with losses which amount to 5 % and 38 % respectively. We note that the corresponding energy losses will be much lower, because the heat diffusivities are much smaller than the particle diffusivities, as shown in Fig. 4, and because particles are lost on average at energies which are close to the critical energy and therefore well below their birth energy.

In Fig. 5(b), the results obtained from the ASTRA simulation of He transport are presented. In the transport simulations, He transport is described by formulae which fit the gyrokinetic results presented in Section 3, namely $D_{He} = \chi_i + \chi_e$ and convective terms given by the solid curves

in Fig. 3. Neoclassical transport is also included, and plays a role inside $\rho_{tor} = 0.1$, where ITG/TEM modes are stable, according to the GLF23 simulation. Two He density profiles are plotted, and compared to the profile of the electron density (renormalised at the same central value). The one plotted in red comes from the solution of the non-homogeneous He transport equation in Eq. (8), and shows the effect of the integral of the He particle source. The one plotted in blue shows the solution of the homogeneous equation, and shows the effect of the He pinch in the absence of source. The latter is very close to the electron density profile obtained by the GLF23 simulation. The actual total He density profile, namely the general steady state solution of the He diffusion equation, is given by a linear combination of these two profiles, where the homogeneous solution can be multiplied by an arbitrary factor which enables the He density to match the value at the boundary. The consequent dependence of the peaking of the He concentration profile as a function of the total He concentration shows that already for total He concentrations as low as 2 %, the He density profile is very close to the electron density profile, with little effect of the He particle source.

6. Conclusions

A general expression for the transport of minority species in small charge concentration has been derived from the nonlinear gyrokinetic equation and shown to be observed by nonlinear gyrokinetic simulations. In nonlinear gyrokinetic simulations, the convection of impurities is usually directed inwards for ion heat fluxes which exceed or are equal to the electron heat flux, but can reverse direction in conditions in which the electron heat flux exceeds significantly the ion heat flux. These results confirm previous linear results. The electrostatic turbulent transport of energetic α particles is computed with both linear and nonlinear gyrokinetic simulations and with both Maxwellian and slowing down unperturbed distribution functions, and found to be negligible in ITER transport modelling. Finally the transport of He ash is investigated, and found to have a convection directed inwards for plasma conditions as those expected in the ITER standard scenario. The He ash diffusivity is large enough to avoid strong accumulation, despite the presence of the central He particle source produced by the α slowing down. The He density profile is predicted to be close to that of the electron density for expected values of the He concentration.

References

[1] Peeters AG, Strintzi D 2004 *Phys. Plasmas* **11** 3748.
[2] Kotschenreuther M *et al* 1995 *Comput. Phys. Commun.* **88** 128.
[3] Dorland W *et al* 2000 *Phys. Rev. Lett.* **85** 5579.
[4] Candy J and Waltz RE 2003 *J. Comput. Phys.* **186** 545.
[5] Candy J and Waltz RE 2003 *Phys. Rev. Lett.* **91** 045001.
[6] Pereverzev G, Yushmanov PN, 2002 *Report IPP* 5/98, Garching.
[7] Waltz RE *et al* 1997 *Phys. Plasmas* **4** 2482.
[8] Frojdh M *et al* 1992 *Nucl. Fusion* **32** 419.
[9] Garbet X *et al* 2005 *Phys. Plasmas* **12** 082511.
[10] Estrada-Mila C *et al* 2005 *Phys. Plasmas* **12** 022305.
[11] Angioni C, Peeters AG 2006 *Phys. Rev. Lett.* **96** 095003.
[12] Dubuit N *et al* 2007 *Phys. Plasmas* **14** 042301.
[13] Angioni C *et al* 2007 *Phys. Plasmas* **14** 055905.
[14] Angioni C *et al* 2007 *Plasma Phys. Controll. Fusion* **49** 2027.
[15] Vlad M, Spineanu F 2005 *Plasma Phys. Controll. Fusion* **47** 281.
[16] Vlad M *et al* 2005 *Plasma Phys. Controll. Fusion* **47** 1015.
[17] Hauff T, Jenko F 2006 *Phys. Plasmas* **13** 102309.
[18] Estrada-Mila C *et al* 2006 *Phys. Plasmas* **13** 112303.
[19] Hauff T, Jenko F 2007 *Phys. Plasmas* **14** 092301.
[20] Dannert T *et al* 2008 *Phys. Plasmas* **15** 062508.
[21] Angioni C, Peeters AG 2008 *Phys. Plasmas* **15** 052307.
[22] Pereverzev GV, Corrigan G 2008 *Comp. Phys. Comm.* doi:10.1016/j.cpc.2008.05.006.
[23] Pereverzev GV *et al* 2005 *Nucl. Fusion* **45** 221.